BIOPHYSICS

Swimming bacteria power microspin cycles

Alex E. Hamby[1], Dhruv K. Vig[1], Sasha Safonova[2], Charles W. Wolgemuth[1,2]*

Dense suspensions of swimming bacteria are living fluids, an archetype of active matter. For example, *Bacillus subtilis* confined within a disc-shaped region forms a persistent stable vortex that counterrotates at the periphery. Here, we examined *Escherichia coli* under similar confinement and found that these bacteria, instead, form microspin cycles: a single vortex that periodically reverses direction on time scales of seconds. Using experimental perturbations of the confinement geometry, medium viscosity, bacterial length, density, and chemotaxis pathway, we show that morphological alterations of the bacteria transition a stable vortex into a periodically reversing one. We develop a mathematical model based on single-cell biophysics that quantitatively recreates the dynamics of these vortices and predicts that density gradients power the reversals. Our results define how microbial physics drives the active behavior of dense bacterial suspensions and may allow one to engineer novel micromixers for biomedical and other microfluidic applications.

INTRODUCTION

Dynamic, biologic systems are often driven by organized forces produced by small constituent molecules or cells. For example, the motion of a neutrophil tracking down a pathogen is powered by directed actin polymerization and myosin contraction (*1–3*). Likewise, the movements of single cells are marshalled together during morphogenesis to properly form an organism (*4–6*). It has become common to call such systems active matter (*7, 8*). A simple model system for studying active matter is a dense suspension of swimming bacteria, where the forces that drive single-cell movements coordinate to generate large-scale fluid flows that lead to complex, and sometimes turbulent, motions (*9–14*). Theoretical investigations into the behavior of active matter have produced semiquantitative agreement with some experiments (*7, 8, 13*); however, we are still only beginning to grasp the range of behaviors possible from even these relatively simple active systems.

Because the internal components of an active system produce force, the system as a whole can spontaneously produce persistent motion without external driving forces. An illustrative example of this effect is seen when dense suspensions of *Bacillus subtilis* (volume fraction > 0.4) are confined in micrometer-scale disc-shaped droplets (*15*). For droplets with diameters between 30 and 70 μm, the bacteria coordinate and flow, creating a single, stable vortex that counterrotates at the periphery (*15*). This stable vortical flow is driven by the forces that the bacteria exert on the surrounding fluid (*16*).

RESULTS

Bacterial microspin cycles

Using a similar experimental assay to that used previously for *B. subtilis*, we examined the dynamics of confined suspensions of *Escherichia coli* (Fig. 1A). *E. coli* and *B. subtilis* are both rod-shaped bacteria that swim using multiple rotating external flagella (*17*). Under standard growth conditions (see Materials and Methods), *E. coli* has a length of 2.83 ± 0.05 μm and a diameter of 1.10 ± 0.01 μm, which is slightly smaller than *B. subtilis*, which has a length of 4.29 ± 0.04 μm and a diameter of 1.70 ± 0.01 μm. The swimming speeds of *E. coli* and *B. subtilis* are also comparable [15 to 25 μm/s (*17*)]. Therefore, it would seem reasonable that the confined dynamics of these bacteria would be similar. Unexpectedly, though, we found that dense suspensions of confined *E. coli* (volume fraction, ~0.56) moved as a periodically oscillating single vortex that changed its direction of rotation approximately every 2 to 4 s (Fig. 1B and movie S1). These periodically reversing motions were found in droplets ranging in size from 20 to 90 μm in diameter. In a given droplet, the period that the vortices switched direction was very regular and, during rotation in a given direction, counterrotation near the periphery was not observed. To quantify the periodicity of the motion, we defined an order parameter for the motion within the droplet as the average of the azimuthal component of the velocity divided by the average magnitude of the velocity, with clockwise flow being defined as positive and counterclockwise flow as negative. The order parameter showed an approximately square wave–like variation in time (Fig. 1C). We also found that the average velocity in the droplet varied periodically at twice the frequency of the order parameter (Fig. 1D). These confined suspensions of bacteria are reminiscent of the spin cycle on a laundry machine, incessantly oscillating between clockwise and counterclockwise motion.

A two-phase continuum model for collective bacterial dynamics

This result raises a number of interesting questions. Why do some bacterial suspensions create vortices with oscillating handedness, while others produce stable flow configurations? What sets the period that the vortices switch direction? While some simulations and active fluid models have reproduced stable vortices in confined bacterial suspensions (*15, 16, 18*) and examined other dynamics that result from confinement (*19, 20*), can any current models explain dynamically switching vortices?

To answer these questions, we began by addressing whether a revised version of our two-phase model for collective bacterial swimming (*21*) was sufficient to explain the periodic flipping observed in *E. coli* droplets. This model considers small volumes of fluid that are large compared to the size of an individual bacterium but smaller than the characteristic length scales of the fluid flows. Averaging over these small regions, the bacterial density is defined by a volume fraction, φ, and the average bacterial velocity is $\mathbf{v}_b$. The fluid moves independently with average velocity $\mathbf{v}_f$. The bacteria interact with the fluid through the forces generated by the rotating flagella (of magnitude F_0), which propel the bacteria at a free-swimming speed of V_0, and resistive drag on the cell body that is proportional to the velocity difference between the fluid and bacteria with resistive drag coefficient ζ_0 (Fig. 2A). These forces are exerted over the length of each bacterium and lead to a net dipole distributed stress on the fluid, with the volume fraction weighted dipole denoted by $\hat{D}$ (Fig. 2B). Averaging over the orientations of the bacteria,

[1]Department of Molecular and Cellular Biology, University of Arizona, Tucson, AZ 85721, USA. [2]Department of Physics, University of Arizona, Tucson, AZ 85721, USA.
*Corresponding author. Email: wolg@email.arizona.edu

a, leads to a closed system of equations defining the dynamics of this system (see the Supplementary Materials for details)

Volume fraction dynamics
$$\frac{\partial \phi}{\partial t} = -\nabla \cdot (\phi \mathbf{v}_b)$$

Force balance on the bacterial phase
$$\underbrace{F_0 \mathbf{a}}_{\text{Thrust force}} - \underbrace{\zeta_0 \phi(\mathbf{v}_b - \mathbf{v}_f)}_{\text{Drag force}} - \underbrace{\frac{\zeta_0 D}{(1-\phi)} \nabla \phi}_{\text{Diffusion}} -$$

$$\underbrace{\phi \nabla P}_{\text{Hydrostatic pressure}} + \underbrace{\eta_b \nabla \cdot (\nabla \mathbf{v}_b + \nabla \mathbf{v}_b^T)}_{\text{Bacterial viscosity}} = 0$$

Force balance on the fluid phase
$$-\underbrace{F_0 \mathbf{a}}_{\text{Thrust force}} - \underbrace{\zeta_0 \phi(\mathbf{v}_f - \mathbf{v}_b)}_{\text{Drag force}} - \underbrace{\zeta_{ex} \mathbf{v}_f}_{\text{Hele-Shaw drag}} - \underbrace{\nabla \cdot (F_0 b D)}_{\text{Dipole-stress}} -$$

$$\underbrace{(1-\phi) \nabla P}_{\text{Hydrostatic pressure}} + \underbrace{\eta_f \nabla \cdot (\nabla \mathbf{v}_f + \nabla \mathbf{v}_f^T)}_{\text{Fluid viscosity}} = 0$$

Orientational dynamics
$$\frac{\partial \mathbf{a}}{\partial t} = -\underbrace{\nabla \cdot (\mathbf{v}_p \mathbf{a})}_{\text{Advection}} - \underbrace{V_0(\nabla \cdot \mathbf{D})}_{\substack{\text{Realignment due} \\ \text{to swimming}}} + \underbrace{D_\psi \nabla^2 \mathbf{a} - g(\phi, \mathbf{a})\mathbf{a}}_{\substack{\text{Diffusion-driven} \\ \text{alignment}}} +$$

$$\underbrace{\mathbf{\tau} \times \mathbf{a}}_{\substack{\text{Torque from} \\ \text{velocity gradients}}}$$

Conservation of volume
$$\nabla \cdot (\phi \mathbf{v}_b + (1-\phi)\mathbf{v}_f) = 0$$

Here, D is an effective diffusion coefficient for the bacteria and b is the dipole length scale, which is approximately equal to the length of the bacterium. The viscosities of the fluid and bacterial phases are η_f and η_b, respectively. Alignment of the bacteria is driven by random motions, with a diffusion coefficient D_ψ and a local, volume fraction–dependent strength $g(\phi, \mathbf{a})$ (Fig. 2C), and there is a torque $\mathbf{\tau}$ that comes from fluid velocity gradients (Fig. 2D).

We found that, for parameters that were appropriate for the morphology and swimming dynamics of *E. coli* (table S1), the model naturally gave rise to periodic reversal of vorticity in simulations that spanned droplets of 30 to 80 μm in diameter (movie S2). The model showed that reversals begin at the edge of the droplet with a small opposite-directed vortex. This counterrotating vortex then sweeps across the droplet until the opposite-directed vortex fills the entire region. Similar behavior is seen in the experiments (movie S1) and is apparent in the second and fourth panels of Figs. 1B and 2E. The dynamics of the order parameter and the average velocity in the droplet matched the basic temporal dynamics observed in the experiments (Fig. 2, F and G).

Confined dynamics has multiple stable states

While the quantitative comparison between the model and experiments provides strong evidence that the relevant physics is accounted for by the mathematical model, it remained unclear what aspect of the physics was controlling the periodic flipping. To unravel these factors, we quantified the flow fields of *E. coli* droplets using optical flow velocimetry
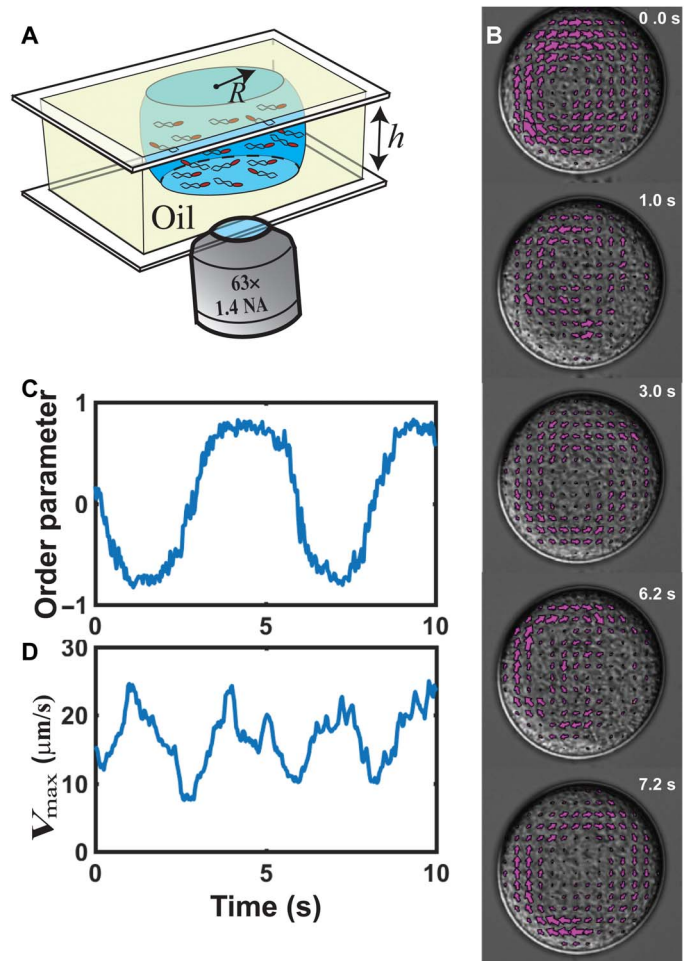
Fig. 1. Dense suspensions of confined *E. coli* form microspin cycles. (A) Schematic of the experimental setup. An emulsion of a bacterial culture and mineral oil is sandwiched between two coverslips. The distance between coverslips is $h \sim 25$ μm. The bacterial culture is confined within roughly disc-shaped droplets of radius R. High-speed differential interference contrast (DIC) microscopy is used to capture the flow of bacteria within the droplet. **(B)** Time sequence of a representative droplet. The flow field is shown with magenta arrows. A single clockwise-rotating vortex at time 3.0 s transitions to a counterclockwise rotating and returns to clockwise rotation at 7.2 s. The average period is approximately 3.4 s, and the droplet is approximately 30 μm in diameter. **(C)** The order parameter (blue line; see text for definition) varies in time as a square wave, providing a quantitative measure of the periodic behavior of the system. **(D)** The maximum velocity in the droplets oscillates in a roughly sawtooth pattern at half the period of the order parameter.

(22). Analysis of more than 200 different droplets revealed four distinct motions: *E. coli*–like (a single vortex that periodically switched directions), *B. subtilis*–like (time-independent vortices with a counterrotating boundary), a stable single vortex, and sporadic motion that did not fall into the other three categories (fig. S1). We then computed the probability for each of these types of motion and used this value as a means for comparing how different parameters, such as cell length, medium viscosity, and volume fraction, affected the behavior of the confined bacteria.

Using wild-type (WT) *E. coli* under standard conditions, we observed periodic flipping in ~70% of the droplets. A smaller fraction of droplets showed either random motions (24%) or a stable single

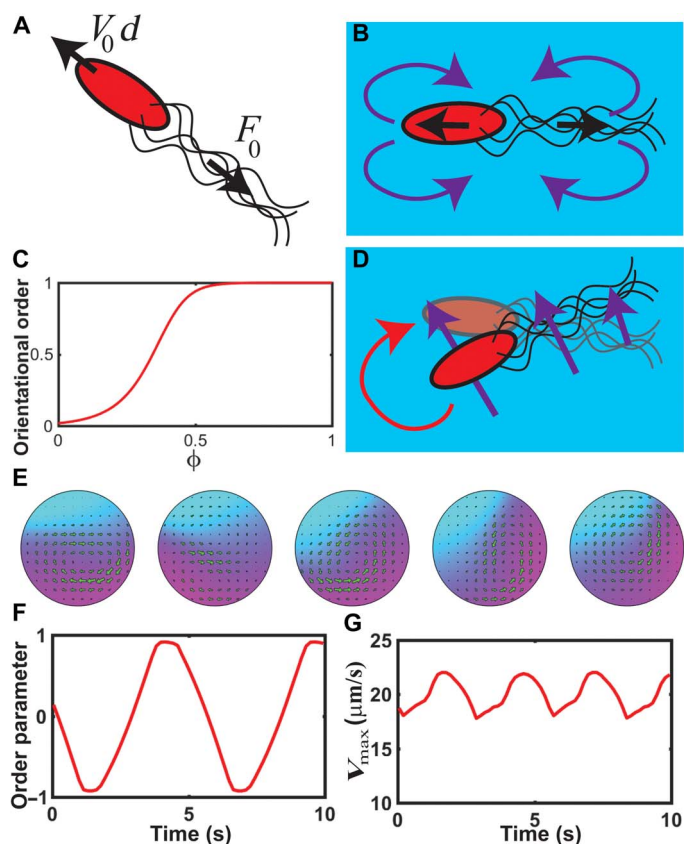**Fig. 2. The two-phase bacterial fluid model recreates the microspin cycles.** (**A**) A free swimming bacterium exerts a thrust force F_0 on the fluid, which causes the bacterium to swim with velocity V_0 in the direction **d**. (**B**) The thrust from the flagella and resistive drag on the entire bacterium (black arrows) produce a dipole-distributed stress on the fluid, which induces a local flow pattern (purple arrows). (**C**) Random movements and hydrodynamic interactions cause the bacteria to align in a volume fraction–dependent manner. We assume an approximately sigmoidal dependence of the orientational order on the volume fraction. (**D**) Gradients of the fluid flow (purple arrows) that are perpendicular to the long axis of the bacteria exert a torque that causes the bacteria to rotate. (**E**) Our mathematical model replicates the behavior observed in Fig. 1B with a slightly faster period (~2.9 s). The color map shows the bacterial volume fraction. (**F**) The simulations reproduce well the dynamics of the order parameter. (**G**) As was observed in the experiments, the maximum velocity in the simulations undulates in a roughly sawtooth-like pattern at half the period of the order parameter.

vortex (6%). We never observed the stable counterrotating vortices that are observed in *B. subtilis* (15). The probability of observing these states was only weakly dependent on droplet size (fig. S2). We observed periodic reversals and random motions in all droplets in the range from 20 to 90 µm in diameter but only observed the stable single vortices in smaller droplets (20 to 45 µm). Droplet diameter did not have any observable effect on the period of the periodically reversing flows.

That droplets under similar conditions show multiple distinct behaviors (periodic reversals, stable vortices, or random motion) suggests that there are multiple stable states of the system. To test whether our mathematical model showed similar behavior, we started simulations with 10 different random initial conditions for the cellular orientation field, leaving all other parameters the same. We found that, in 60% of the simulations, periodic reversals resulted, while a single constant vortex was observed the other 40% of the time (movie S2). While the mathematical model did not lead to random motions, it does show

that the model naturally includes bistability reminiscent of what is observed experimentally.

Bacterial length controls the ability to form microspin cycles

Because cell body length is perhaps the most notable physical difference between *B. subtilis* and *E. coli*, we used the β-lactam antibiotic cephalexin to probe the effects of body length on the fluid flows produced by confined *E. coli*. By blocking cell division, cephalexin produces long filamentous cells (23, 24), and incubation time can be used to controllably modulate cell length up to 7.1 µm. The probability of a given flow pattern was quantified in droplets for bacteria with six different lengths (Fig. 3A). *B. subtilis*–like flow in *E. coli* droplets emerged for lengths greater than 2.8 µm and predominated at large cell body lengths (Fig. 3, A and B). For these stable vortical flows, we found that the velocity has a maximum at a specific radial position and that this peak increases and shifts as cell length is increased (Fig. 3C). However, while body length affected the ability of *E. coli* to periodically reverse direction, it did not affect the periodicity: The half-period of reversals was unaffected by cell body length (Fig. 3D). This suggests that longer cells sterically hinder each other from flipping around but that cell length does not directly influence the rate of flipping.

To account for bacterial length effects in the model, we assumed that a number of parameters were proportional to the length, specifically, the dipole length scale, the effective viscosity of the bacterial phase, and the strength of the diffusion-driven alignment term. Varying the length of the bacteria in the simulations correctly predicted a very weak dependence of the half-period on bacterial length (~10% variation for lengths between 2.5 and 7.0 µm; fig. S3). The model did not show a complete loss of reversals at lengths greater than 6.0 µm as we observed experimentally, but it did show a maximum reversal probability for bacteria of length 4.0 µm (fig. S3). The model also showed moderate differences in the average velocity with bacterial length. In stable vortices, the velocity increased with length, whereas for periodic reversing droplets the average velocity decreased with length (fig. S3).

Run-and-tumble behavior does not affect microspin cycle dynamics

We also studied the requirement for tumbling. While *E. coli* and *B. subtilis* cells tumble approximately every 3 s, individual *E. coli* cells are more likely to tumble than *B. subtilis* (17). We, therefore, examined the nontumbling, chemotaxis-gutted *E. coli* strain RBB1050 (25) and found that it still produced periodic fluid flows with a comparable period to the WT cells (half-period, $T_{1/2} = 4.6 \pm 2$ s) (fig. S4), thereby ruling out tumbling as a requirement for periodic flow.

Viscosity and volume fraction affect the likelihood of flow reversal

Other parameters were found to affect the likelihood of periodic reversals in dense *E. coli* droplets, such as medium viscosity and bacterial volume fraction. The fraction of periodic droplets was maximum when the bacterial volume fraction was 0.56 (fig. S5). Increasing medium viscosity reduced the fraction of periodic flows, and 10% Ficoll led to full extinction of periodic droplets (fig. S6). However, neither of these parameters altered the frequency of reversal (Fig. 3, E and F).

What then sets the reversal frequency?

We hypothesized that the time scale defined by the ratio of droplet diameter to velocity may contribute to the value of $T_{1/2}$, as it is comparable to our measured half-periods, because the average maximum flow
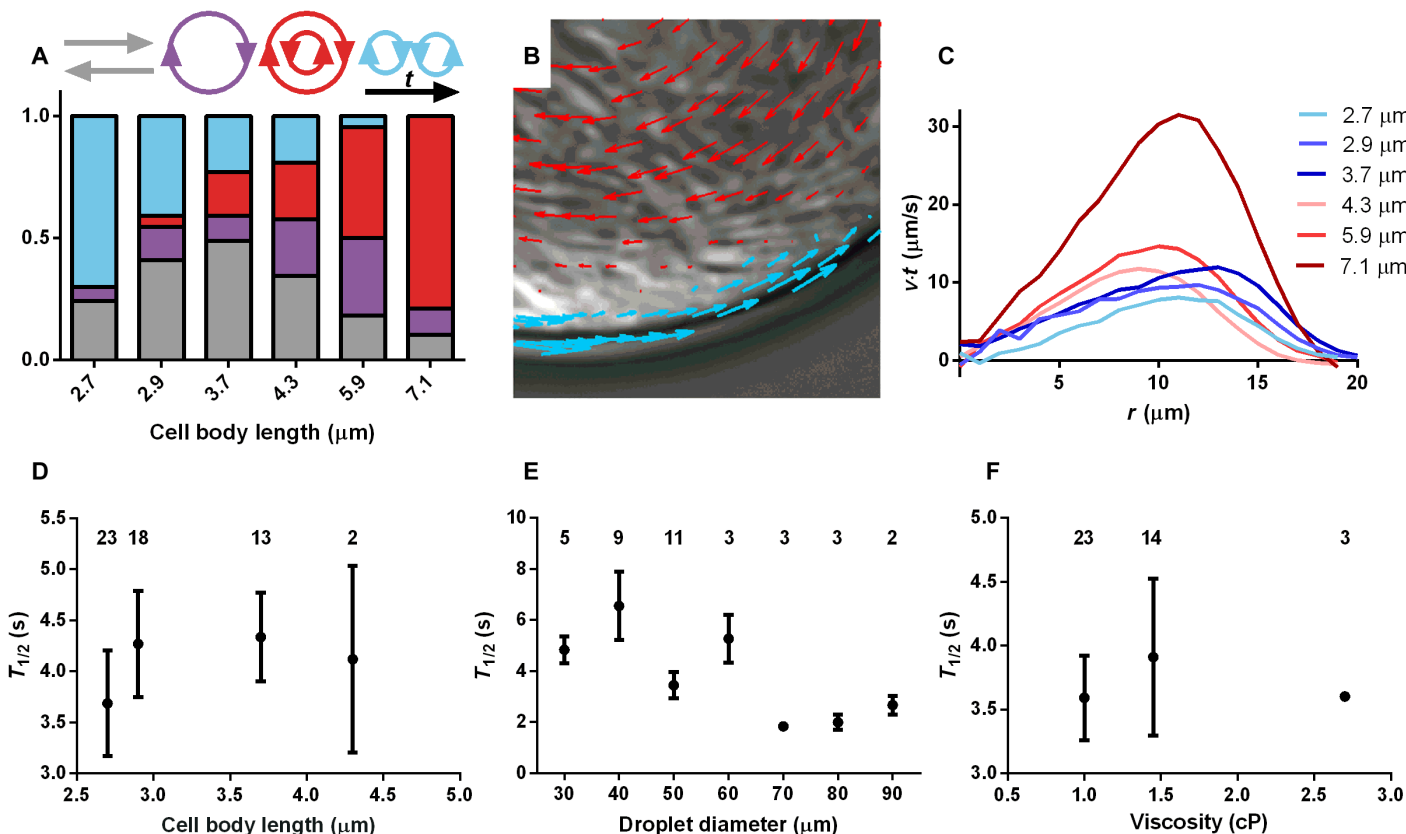
Fig. 3. Length modulates flow pattern. (**A**) As cell body length increases, the probability of observing different flow patterns changes from that of *E. coli*–like, periodic reversals (blue) to *B. subtilis*–like, stable vortices (red). Sporadic droplets (gray) are more common at transitional lengths, and single vortices (purple) are uncommon across all lengths. (**B**) Flow field of a droplet containing 5.9-μm-long *E. coli*, showing a flow pattern with counterrotation at the boundary (light blue), reminiscent of the flows produced by *B. subtilis*. The counterflow arrows are not drawn to scale. (**C**) Azimuthal velocity as a function of radial position. Counterrotation at the periphery increases with cell length, and the location of the peak velocity shifts inward toward the center of the droplet. The half-period of periodically reversing *E. coli* droplets does not depend on (**D**) bacterial cell length, (**E**) droplet diameter, or (**F**) medium viscosity. (D to F) Numbers above the data points are the sample size. (E) Data points represent the average value for droplets with diameters within ±5 μm of the data point. The correlation between the half-period and the diameter (E) is not significant ($P > 0.9$). Error bars show SEM.

velocity was ~25 μm/s for WT droplets with diameters of ~20 μm. In addition, because the maximum velocity in the droplets is proportional to the droplet diameter and independent of the volume fraction (Fig. 4, A and B), we would expect the half-period to be independent of these parameters, as observed. One way to modify the collective speed of the bacteria in the droplets is to alter the swimming speed of the individual cells. We found that bacteria in late log phase swim substantially slower than those at mid-log phase. By selecting bacteria from different phases in growth, we were able to adjust swimming speeds from 6 to 13 μm/s (fig. S7). Consistent with our hypothesized scaling, we found that the half-period varied inversely to the cell velocity (Fig. 4B). Cell velocity did not strongly affect the probabilities of observing reversals (fig. S2B).

Density gradients drive reversals

While the swimming speed of individual cells affects the period of the oscillations, it remained unclear what physical mechanism drives the reversals. In our simulations, we found that random initial conditions that produced periodic reversals also had an asymmetric density distribution of bacteria within the droplet, whereas initial conditions that led to stable vortical motion had an azimuthally symmetric density distribution (Fig. 4, C and D). To test whether this same distribution is

observed experimentally, we used the membrane dye FM 4-64 to fluorescently stain the bacteria and observed asymmetric fluorescence in droplets that showed reversals, while droplets with random motion or stable vortices had symmetric fluorescence intensity with a peak in fluorescence at the edge of the droplet (Fig. 4, E and F, and movie S5). Therefore, the density gradient is likely the driving force for creating these periodic reversals, which is consistent with the proposal that random motion of the bacteria leads to an effective torque when the bacterial orientation is perpendicular to the gradient of the density (21).

DISCUSSION

Here, we have shown that dense suspensions of *E. coli* produce notable periodic reversals when confined in small regions. Using an exhaustive array of experiments, we varied key parameters in the system to determine what physics drives these reversals, especially considering that *B. subtilis* does not show this behavior. We found that cell length is a dominant factor in controlling the propensity for periodic flows but has little to no effect on the reversal frequency. Because cell length does not affect the reversal frequency, this result suggests that cell length may not be a driving factor in producing the reversals, but rather, because longer cells are harder to rotate and more likely to collide with one another in a
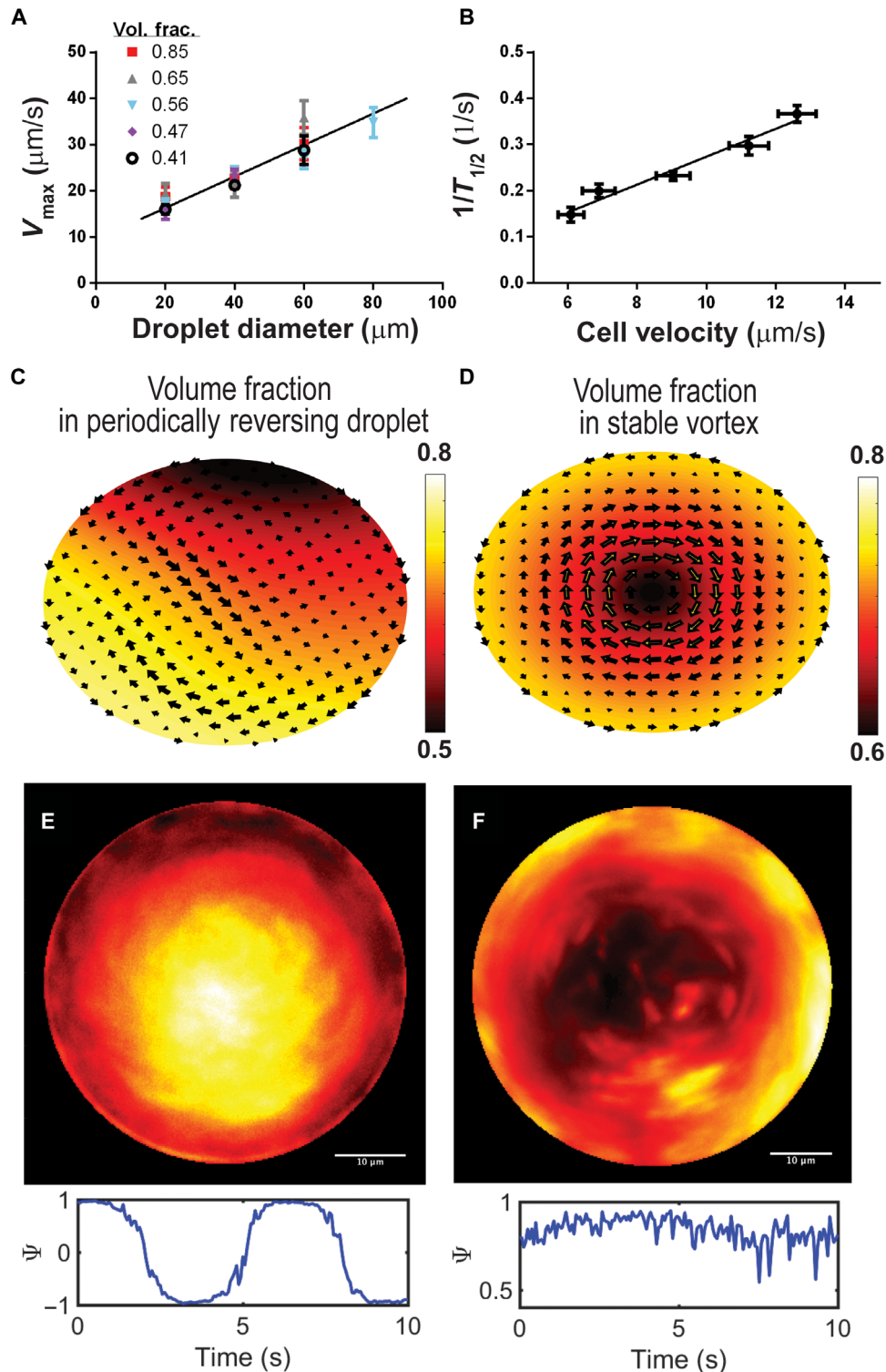
Fig. 4. Dependence of reversals on diameter, swimming speed, and density distribution. (**A**) Flow velocity depends linearly on droplet diameter and does not depend strongly on volume fraction. Data points represent the average value and SEM for droplets with diameters within ±10 μm of the data point. (**B**) The inverse of the half-period scales linearly with the swimming speed of the bacteria. The simulations predict that there is an asymmetric density distribution for droplets that periodically reverse (**C**), whereas the distribution is symmetric for droplets with stable vortices (**D**). The color map in (C) shows the volume fraction of the bacteria. FM 4-64 was used to fluorescently stain the bacterial membranes. Images represent the fluorescent intensity in the droplets averaged over 1 s for a droplet undergoing periodic reversals (**E**) and one undergoing stable vortical motion (**F**). The color maps in (E) and (F) are in arbitrary units. The plots underneath the images show the order parameter (Ψ) versus time for these droplets. Scale bars, 10 μm.

dense, locally aligned suspension, cells with longer lengths may just prevent each other from being able to reverse direction. Average cell swimming speed, on the other hand, was the only control parameter that altered frequency, which suggests that the frequency is proportional to the single-cell speed divided by the diameter of the droplet. Notably, the observed flows are apparently multistable: Under similar conditions, we observed different types of flows in a droplet, periodically reversing, stable vortices, or random motions. Our two-phase mathematical model for collective motion of bacteria showed quantitative agreement with our experiments and also suggests a mechanism for the multistable behavior. Specifically, the multistable behavior is dependent on establishing an asymmetric density gradient across the droplet.

The results presented here provide new insights into the behavior and physics of active systems. We have shown that subtle changes in the physical properties of a dense suspension of swimming bacteria can lead to major qualitative changes in the dynamics of the system. While at face value this finding would seem to suggest that even simple active systems are substantially complex, we found that a model that encompasses the basic physical aspects of this system is predictive for how minor geometrical differences switch a stable vortex of confined bacteria into one that periodically oscillates. This work is then suggestive that active suspensions can be designed to achieve specific tasks. One such application of the work presented here is in the field of micromixing, which is currently an active area of microfluidic design for a range of biomedical and other microfluidic applications, such as polymerization, DNA analysis, enzyme screening, and the detection and analysis of chemical or biochemical content (26–28). Chemical transport and reactions that occur in microvolumes typically rely on slow diffusive processes. Passive or active mixing accelerates these processes by bringing soluble chemicals together more rapidly than pure diffusion. The modeling and experiments that we describe here can provide a means to custom design active matter systems to produce micromixers that meet specific protocol requirements.

MATERIALS AND METHODS
Cell culture
WT strain MG1655 was grown in standard Terrific Broth (TB; Sigma) at 37°C and shaken at 200 rpm. An overnight culture was started from a frozen glycerol stock and was diluted 200× and grown for 5 hours until late-exponential phase [optical density at 600 nm (OD_{600}) of 0.6 ± 0.05].

Chemotaxis-gutted *E. coli* mutant RBB1050 (gift of R. Bourret, University of North Carolina) was grown in standard Tryptone Broth (TrB) supplemented with streptomycin (50 μg/ml; Sigma) for selection and shaken at 200 rpm. An overnight culture was grown from a frozen glycerol stock derived from a clonal population of nonchemotactic cells and was diluted 200× and grown for 6 hours to late-exponential phase (OD_{600} of 0.4 ± 0.05).

To alter the average length of the *E. coli* cells, cephalexin (60 μg/ml) was added during the last 20 min to 2 hours of growth. To compute the average cell length for a given incubation time in cephalexin, still images were acquired using DIC microscopy and a 63×/1.4 numerical aperture (NA) objective at low cell densities. Using the image analysis software ImageJ (29), we measured the length of 200 to 400 individual cells for each cephalexin condition.

To alter the viscosity of the bacterial medium, a 20% stock solution of Ficoll PM-400 (Sigma) was prepared in TB by slowly dissolving 10 g of Ficoll powder in TB until reaching a final volume of 50 ml. This solution was filter sterilized and diluted with sterile TB to produce homo-geneous solutions of the desired concentrations (5 to 10%). Solutions were stored at 4°C until time of imaging.

A quantity of 10 ml of stock solution was added to a No. 2 size Gilmont falling ball viscometer (Thermo Fisher Scientific, Waltham, MA) as per the manufacturer's instructions. A glass bead was used for lower viscosity solutions (2 to 20 cP), and a stainless steel bead was used for higher viscosities (10 to 100 cP). The time required for the bead to drop a fixed distance was recorded. Three trials were performed for each sample, and the average time, t, was used to calculate the viscosity, μ, as per the following formula

$$\mu = K(\rho_c - \rho)t$$

where K is a constant, ρ_c is the density of the bead, and ρ is the density of the solution. The drop time for the bead in water, which was assumed to have a viscosity of 1 cP, was used to determine the value of K. The same method was used to measure the viscosity of TB without Ficoll. We found that TB has a viscosity comparable to water.

Slide preparation
Slides were prepared following the procedure described in (15). Five milliliters of cell culture was centrifuged for 10 min at 2000g. Medium was poured from the tube, and the pellet was dried. The pellet was then gently resuspended (carefully avoiding scratching the pellet with the pipette tip) in TB, TB-Ficoll stock, or TrB. D-Mannose (RPI Corp.) was added to TrB for RBB1050 resuspension medium at a final concentration of 0.2% to prevent bacteria from clumping together. The volume of medium used to resuspend the pellet ranged from 0 to 50 μl to modulate volume filling fractions from 0.85 to 0.41. Twenty-five microliters of volume fraction–adjusted culture was transferred to a 1.5-ml microcentrifuge tube. An emulsion was created by pipetting and mixing the culture with 100 μl of mineral oil (Sigma) containing diphytanoyl phosphatidylcholine (DiPhyPC; 10 mg/ml; Avanti) to prevent droplets from coalescing. The microcentrifuge tube was then rolled, upright, between thumb and forefinger for ~10 s to create a gradient in droplet size across the height of the tube. Fifteen microliters of emulsion was pipetted from the top of the tube, to select for small droplets, and was sandwiched between two coverslips. Coverslips were rendered hydrophobic with silane (Sigma) ~1 hour before imaging to create droplets that were widest equidistant from the coverslips. This method produced many pancake-shaped droplets with heights of approximately 25 μm and diameters from 10 to 200 μm.

Because oxygen consumption by the bacteria limits the amount of time droplets remain motile (15), the time between all steps of slide preparation was minimized and monitored carefully. Setting time = 0 at the completion of centrifugation, the pellet was dried and resuspended until time = 60 s. Emulsion pipetting then lasted until time = 120 s. Slides were plated and rushed to the prepared microscope to be imaged immediately.

Volume fraction, ϕ, was calculated as per the following formula

$$\phi = \frac{\phi_0}{1 + d/V_0}$$

where ϕ_0 is the volume fraction of the pellet, V_0 is the pellet volume, and d is the volume of fluid in which the pellet was resuspended. Using the maximum packing density of circles, 0.9, to set an upper limit to our estimate, we estimated the value of ϕ_0 to be 0.85. Using a pipette, V_0

was measured for three *E. coli* and three *B. subtilis* cultures. V_0 for *B. subtilis* was 56 ±14 μl and for *E. coli* was 47± 2 μl. Volume fraction was then modulated by changing d during slide preparation.

Microscopy and image processing

All movies were acquired at 32 frames per second (fps) on a Zeiss Axio Observer inverted microscope equipped with a Hamamatsu ORCA-Flash4.0 CMOS camera. Movies were captured with a 63× oil immersion objective (1.4 NA), focused equidistant from coverslips. All movies were either DIC or wide-field fluorescence using Zeiss Filter Set 43 (HE DsRed). Slides were discarded after 3 min on the microscope (5.5 min after centrifugation ends), before oxygen consumption led to oxygen gradient formation and altered cell motility.

In general, video microscopy images were acquired for 30 s. These images were used to determine the probability that the bacteria would undergo periodic reversals and to determine the characteristics of the velocity fields, such as maximum velocity, average velocity, and the velocity as a function of radial position. For conditions where periodic reversals were not observed (i.e., cephalexin-treated cells that were longer than 6 μm), some 10-s videos were used to quantify the flow characteristics.

Droplet velocity fields were calculated by defining the region of interest about a droplet using a custom MATLAB algorithm to threshold a given droplet region in each frame of a time-lapse movie. This sequence of binary masks was then used along with a gradient-based optical flow method (22) to determine the velocity fields. The velocity fields were validated by simulating the motion of virtual tracer particles in the computed flow, as described in (22).

Flow patterns in the droplets were classified using the dynamics of the order parameter ψ as a metric (fig. S1). Plots of ψ versus time that showed periodicity (which was almost always a square wave shape) were classified as periodic reversals. When the magnitude of ψ was >0.5 for the length of the movie and did not change sign, the droplet was classified as a stable vortex. These droplets were further classified as either a single stable vortex or a counterrotating vortex based on whether or not the optical flow–extracted velocity fields had counter flow at the edge of the droplet. All droplets that were not classified as any of these patterns were categorized as showing random motion.

The half-period ($T_{1/2}$) was measured by hand using the order parameter versus time plots. These plots were opened in ImageJ (29), and the time it took to go from one handedness of flow (e.g., counterclockwise) to the other (e.g., clockwise) was measured for each transition. The half-period was defined as the average value of these measurements.

Bacterial density measurements

Cultures were stained with 4 μM FM 4-64 (Life Technologies) for 20 min and were then centrifuged and pelleted as above. After removal of the supernatant, the bacteria were resuspended in 25 μl of TB. Droplets were created by pipetting and mixing the culture with 100 μl of mineral oil with DiPhyPC and were sandwiched between silane-coated coverslips. For each droplet, a 10-s DIC movie was captured, immediately followed by a 10-s epifluorescence movie. Each of these movies was acquired at a rate of 16 fps with 2 × 2 binning.

Average fluorescence intensity was determined within droplets using the ImageJ Z-project tool to average the intensity over a specific length of time (typically 1 s). To confirm asymmetry in the intensity distribution, the plot profile tool was used to measure the intensity across two perpendicular cuts through each averaged fluorescent image.

Single-cell velocities

E. coli was grown for 5 to 7 hours, centrifuged, and resuspended in TB at low volume fraction before being plated in tunnel slides constructed using two layers of double-sided tape as spacers between slide and coverslip. Ten-second DIC movies were taken as described above. Individual cells were identified in our images using nonnegative mixed-norm preconditioning (30) to threshold the images. The resulting binary images were then used to track the center of mass for individual cells, and the instantaneous velocity was computed as the difference in center of mass position between successive frames. The instantaneous velocity was then averaged for each cell individually.

SUPPLEMENTARY MATERIALS

Supporting Methods

Fig. S1. Characteristic dynamics of the order parameter for representative droplets.

Fig. S2. The effect of droplet diameter and cell swimming speed on the probability of different flow patterns.

Fig. S3. Model predictions for the effect of bacterial length on the flow dynamics.

Fig. S4. Counterrotations are not affected by *che* mutants.

Fig. S5. The effect of volume fraction on the probability of different flow patterns.

Fig. S6. The effect of fluid viscosity on the probability of different flow patterns.

Fig. S7. The effect of growth time on single-cell velocities.

Table S1. Model parameters.

Movie S1. Confined *E. coli* forms microspin cycles.

Movie S2. Simulations of our two-phase model for collective motion of bacteria predict two types of flows for a given set of parameters, either periodic reversals or stable vertical flow, which depend on the initial conditions.

Movie S3. *E. coli* cells treated with cephalexin are longer and, for cells over 3.0 μm in length, will produce counterrotating vortices reminiscent of *B. subtilis*.

Movie S4. Confined *E. coli* mutants form microspin cycles.

Movie S5. The bacterial membranes were stained with the fluorescent dye FM 4-64.

References (31–37)

REFERENCES AND NOTES

1. H. Saito, Y. Minamiya, S. Saito, J.-i. Ogawa, Endothelial Rho and Rho kinase regulate neutrophil migration via endothelial myosin light chain phosphorylation. *J. Leukoc. Biol.* **72**, 829–836 (2002).

2. K. M. Stroka, H. N. Hayenga, H. Aranda-Espinoza, Human neutrophil cytoskeletal dynamics and contractility actively contribute to trans-endothelial migration. *PLOS ONE* **8**, e61377 (2013).

3. M. Affolter, C. J. Weijer, Signaling to cytoskeletal dynamics during chemotaxis. *Dev. Cell* **9**, 19–34 (2005).

4. E. Theveneau, B. Steventon, E. Scarpa, S. Garcia, X. Trepat, A. Streit, R. Mayor, Chase-and-run between adjacent cell populations promotes directional collective migration. *Nat. Cell Biol.* **15**, 763–772 (2013).

5. E. Scarpa, R. Mayor, Collective cell migration in development. *J. Cell Biol.* **212**, 143–155 (2016).

6. A. Aman, T. Piotrowski, Cell migration during morphogenesis. *Dev. Cell* **341**, 20–33 (2010).

7. S. Ramaswamy, The mechanics and statistics of active matter. *Annu. Rev. Condens. Matter Phys.* **1**, 323–345 (2010).

8. M. C. Marchetti, J. F. Joanny, S. Ramaswamy, T. B. Liverpool, J. Prost, M. Rao, R. A. Simha, Hydrodynamics of soft active matter. *Rev. Mod. Phys.* **85**, 1143–1189 (2013).

9. C. Dombrowski, L. Cisneros, S. Chatkaew, R. E. Goldstein, J. O. Kessler, Self-concentration and large-scale coherence in bacterial dynamics. *Phys. Rev. Lett.* **93**, 098103 (2004).

10. A. Sokolov, I. S. Aranson, J. O. Kessler, R. E. Goldstein, Concentration dependence of the collective dynamics of swimming bacteria. *Phys. Rev. Lett.* **98**, 158102 (2007).

11. J. Dunkel, S. Heidenreich, K. Drescher, H. H. Wensink, M. Bär, R. E. Goldstein, Fluid dynamics of bacterial turbulence. *Phys. Rev. Lett.* **110**, 228102 (2013).

12. S. D. Ryan, A. Sokolov, L. Berlyand, I. S. Aranson, Correlation properties of collective motion in bacterial suspensions. *New J. Phys.* **15**, 105021 (2013).

13. A. Morin, D. Bartolo, Flowing active liquids in a pipe: Hysteretic response of polar flocks to external fields. *Phys. Rev. X* **8**, 021037 (2018).

14. H. Wioland, E. Lushi, R. E. Goldstein, Directed collective motion of bacteria under channel confinement. *New J. Phys.* **18**, 075002 (2016).

15. H. Wioland, F. G. Woodhouse, J. Dunkel, J. O. Kessler, R. E. Goldstein, Confinement stabilizes a bacterial suspension into a spiral vortex. *Phys. Rev. Lett.* **110**, 268102 (2013).

16. E. Lushi, H. Wioland, R. E. Goldstein, Fluid flows created by swimming bacteria drive self-organization in confined suspensions. *Proc. Natl. Acad. Sci. U.S.A.* **111**, 9733–9738 (2014).

17. L. Turner, L. Ping, M. Meubauer, H. C. Berg, Visualizing flagella while tracking bacteria. *Biophys. J.* **111**, 630–639 (2016).

18. X. Yang, D. Marenduzzo, M. C. Marchetti, Spiral and never-settle patterns in active systems. *Phys. Rev. E* **89**, 012711 (2014).

19. M. Paoluzzi, R. Di Leonardo, L. Angelani, Self-sustained density oscillations of swimming bacteria confined in microchambers. *Phys. Rev. Lett.* **115**, 188303 (2015).

20. T. N. Shendruk, A. Doostmohammadi, K. Thijssem, J. M. Yeomans, Dancing dislocations in confined active nematics. *Soft Matter* **13**, 3853–3862 (2017).

21. C. W. Wolgemuth, Collective swimming and the dynamics of bacterial turbulence. *Biophys. J.* **95**, 1564–1574 (2008).

22. D. K. Vig, A. E. Hamby, C. W. Wolgemuth, On the quantification of cellular velocity fields. *Biophys. J.* **110**, 1469–1475 (2016).

23. D. Greenwood, F. O'Grady, Comparison of the responses of *Escherichia coli* and *Proteus miarbilis* to seven β-lactam antibodies. *J. Infect. Dis.* **128**, 211–222 (1973).

24. G. N. Rolinson, Effect of β-lactam antibiotics on bacterial cell growth rate. *J. Gen. Microbiol.* **120**, 317–323 (1980).

25. W. N. Abouhamad, D. Bray, M. Schuster, K. C. Boesch, R. E. Silversmith, R. B. Bourret, Computer-aided resolution of an experimental paradox in bacterial chemotaxis. *J. Bacteriol.* **180**, 3757–3764 (1998).

26. G. S. Jeong, S. Chung, C.-B. Kim, S.-H. Lee, Applications of micromixing technology. *Analyst* **135**, 460–473 (2010).

27. J. M. Ottino, S. Wiggins, Designing optimal micromixers. *Science* **305**, 485–486 (2004).

28. C.-Y. Lee, L.-M. Fung, Recent advances and application of micromixers. *Sens. Actuators B Chem.* **259**, 677–702 (2018).

29. C. A. Schneider, W. S. Rasband, K. W. Eliceiri, NIH Image to ImageJ: 25 years of image analysis. *Nat. Methods* **9**, 671–675 (2012).

30. K. Li, T. Kanade, Nonnegative mixed-norm preconditioning for microscopy image segementation. *Inf. Process. Med. Imaging* **21**, 362–373 (2009).

31. O. S. Pak, E. Lauga, Theoretical models in low-Reynolds-number locomotion, in *Fluid-Structure Interactions in Low-Reynolds-Number Flows*, C. Duprat, H. A. Stone, Eds. (Royal Society of Chemistry, 2015).

32. M. Doi, S. F. Edwards, *The Theory of Polymer Dynamics* (Oxford Univ. Press, 1986).

33. I. S. Aranson, A. Sokolov, J. O. Kessler, R. E. Goldstein, Model for dynamical coherence in thin films of self-propelled microorganisms. *Phys. Rev. E* **75**, 040901 (2007).

34. N. G. Cogan, R. D. Guy, Multiphase flow models of biogels from crawling cells to bacterial biofilms. *HFSP J.* **4**, 11–25 (2010).

35. H. C. Berg, *Random Walks in Biology* (Princeton Univ. Press, ed. 2, 1993).

36. R. E. Goldstein, A. I. Pesci, M. J. Shelley, Instabilities and singularities in Hele–Shaw flow. *Phys. Fluids* **10**, 2701 (1998).

37. C. W. Wolgemuth, M. Zajac, The moving boundary node method: A level set-based, finite volume algorithm with applications to cell motility. *J. Comput. Phys.* **229**, 7287–7308 (2010).

Citation: A. E. Hamby, D. K. Vig, S. Safonova, C. W. Wolgemuth, Swimming bacteria power microspin cycles. *Sci. Adv.* **4**, eaau0125 (2018).

Science Advances

Swimming bacteria power microspin cycles

Alex E. Hamby, Dhruv K. Vig, Sasha Safonova and Charles W. Wolgemuth

ARTICLE TOOLS	http://advances.sciencemag.org/content/4/12/eaau0125
SUPPLEMENTARY MATERIALS	http://advances.sciencemag.org/content/suppl/2018/12/17/4.12.eaau0125.DC1
REFERENCES	This article cites 34 articles, 4 of which you can access for free http://advances.sciencemag.org/content/4/12/eaau0125#BIBL
PERMISSIONS	http://www.sciencemag.org/help/reprints-and-permissions

Use of this article is subject to the Terms of Service